(Received 2 December 2024, Accepted 10 February 2025, Scheduled 17 February 2025)

A Review of DOA Estimation Technology Based on Programmable Metasurfaces

Zhicheng Pei[1,2], Tong An[1], Peixuan Zhu[1,3,4], and Huan Lu[1,3,4,*]

[1]State Key Laboratory of Extreme Photonics and Instrumentation
ZJU-Hangzhou Global Scientific and Technological Innovation Center
Zhejiang University, Hangzhou 310027, China
[2]No. 36, Institute of CETC, Jiaxing 314001, China
[3]International Joint Innovation Center
The Electromagnetics Academy at Zhejiang University, Zhejiang University, Haining 314400, China
[4]Key Lab. of Advanced Micro/Nano Electronic Devices & Smart Systems of Zhejiang
Jinhua Institute of Zhejiang University, Zhejiang University, Jinhua 321099, China

ABSTRACT: High-precision Direction of Arrival (DOA) estimation requires the use of a large-scale antenna array to achieve accurate results. However, the increasing number of antennas brings substantial challenges that hinder the practical implementation of DOA estimation in real-world engineering applications. The complexity and cost associated with deploying extensive antenna systems can be prohibitive. In contrast, digital metasurfaces offer a promising solution by dynamically manipulating electromagnetic waves. These advanced surfaces enable precise control over wavefronts while utilizing significantly fewer elements, leading to a more compact and cost-effective approach without sacrificing the high-resolution capabilities necessary for effective DOA estimation. This innovative technology not only simplifies the design but also enhances performance. To provide insights for future advancements in this field, this paper reviews the current research status of various DOA estimation techniques that integrate metasurfaces with conventional wave-direction estimation systems, highlighting their potential and applications in improving DOA estimation accuracy.

1. INTRODUCTION

Direction-of-Arrival (DOA) estimation refers to the technique used to determine the direction from which a signal, typically radio waves or sound waves, arrives at a sensor or array of sensors. This technology plays a critical role in various fields such as communications, radar systems, sonar, and wireless networks [1]. Various wave-direction measurement technologies are employed in engineering fields, including Watson-Watt direction finding technology [2], interferometer direction finding systems [3], and Doppler direction finding methods [4]. However, these methods suffer from low angular resolution and are significantly affected by multipath effects. Advanced algorithms like MUSIC (Multisignal Classification) [5] and ESPRIT (Estimation of Signal Parameters via Rotational Invariant Techniques) [6] improve performance but require complex hardware setups, significant computational resources, and are costly. These algorithms typically depend on array antennas, further complicating the hardware architecture. Compressive sensing (CS) [7] has emerged as an effective alternative for DOA estimation. CS leverages the sparsity of signal direction in the spatial domain, employing sparse recovery algorithms like Basis Pursuit and Orthogonal Matching Pursuit (OMP) [8, 9]. This method can estimate the incident signal's direction with fewer measurements, overcoming many limitations of traditional algorithms. However, it still requires large array antennas and multiple independent RF (radio frequency) receiving channels to capture amplitude or phase data, making the system bulky and expensive. Multibeam lens systems, known for their low cost, wide-angle scanning, and simple structure, face challenges due to the difficulty in processing dielectric materials, restricting their application in direction-finding systems [10].

Recently, metasurface-based DOA estimation methods have been developed to address these issues, such as the difficulty of processing and the high purity requirements of dielectric materials. Electromagnetic (EM) metasurfaces are artificial structures made up of subwavelength elements arranged periodically or non-periodically. These surfaces can regulate the magnitude, phase, or polarization of EM waves by manipulating the size and arrangement of the elements to implement different functions such as DOA estimation [5, 11, 12], holographic imaging [13, 14], and electromagnetic focus [15–20]. Metasurfaces are typically single-layered or composed of a few cascaded layers, offering low profile, ease of fabrication [21], and light weight. These characteristics contribute to the miniaturization and integration of DOA systems.

Digital programmable metasurfaces, consisting of numerous digital elements, can dynamically reconstruct EM functions across space, time, and frequency domains [22]. They are widely used in adaptive beams [23–30], communication systems [31–33], stealth technology [34–39], holographic imaging [13, 14], and intelligent sensing [40–44]. The reconfig-

* Corresponding author: Huan Lu (luhuan123@zju.edu.cn).

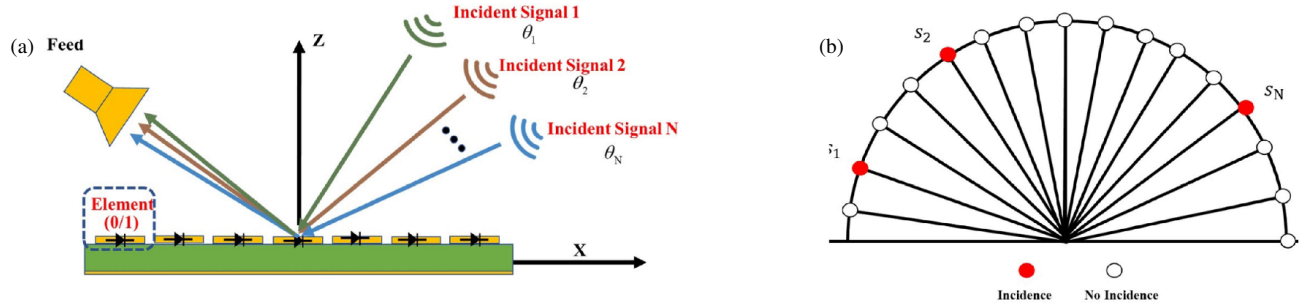

FIGURE 1. (a) Space-fed tunable metasurface sensor for direction of arrival estimation. (b) Sparse representation of incoming signals [47]. Figures reproduced from: Ref. [47], Copyright 2021, IEEE.

urable nature of these metasurfaces significantly reduces the number of required RF receiving channels for DOA estimation [45, 46], simplifying the system structure and lowering costs. Thus, digital programmable metasurfaces provide an ideal hardware platform for high-performance DOA estimation.

This study provides a comprehensive review of the design, structure, and characteristics of various metasurfaces employed for DOA estimation. By examining a range of innovative metasurface technologies, the analysis emphasizes their unique advantages over traditional methods. Metasurfaces, with their ability to manipulate electromagnetic waves at subwavelength scales, offer significant improvements in resolution, flexibility, and efficiency. This review not only highlights the advancements in metasurface design but also explores their potential to overcome the limitations commonly associated with conventional DOA estimation techniques. By showcasing these benefits, the study aims to underscore the transformative impact of metasurfaces on the field of DOA estimation, paving the way for future research and practical applications in this rapidly evolving area.

2. METASURFACES FOR DOA ESTIMATION

2.1. DOA Estimation Based on Digital Coding Metasurfaces

In 2021, Lin et al. [47] proposed a method that used a tunable metasurface to create a random radiation pattern as the physical random-sampling sensing unit for incident signal. In this method, only one radio frequency receiving channel can be used to obtain the CS measurement matrix, and Orthogonal Matching Pursuit algorithm is then applied to realize DOA estimation. The receiving system is composed of a programmable metasurface and horn antenna feeder as depicted in Figure 1. Assume that N signals from various directions $(\theta_1, \theta_2, \cdots, \theta_N)$ are effecting the metasurface by the far-field condition. The metasurface's configuration code matrix is denoted as $B \in Z^{1\times M}$. The signal received by the horn antenna at t_i for a particular metasurface coding matrix B can be expressed as

$$x(t_i) = \sum_{n=1}^{N}\sum_{m=1}^{M} s_n e^{-j\varphi_{ni}}(-1)^{B_m} e^{-j\frac{2\pi}{\lambda}(x_m \sin\theta_n)+j\frac{2\pi}{\lambda}\sqrt{z_f^2+(x_f-x_m)^2}} + n(t_i), \quad (1)$$

In Equation (1), φ_i denotes the phase value at time t_i for the n^{th}; $n(t_i)$ represents the Gaussian noise; σ^2 is the power intensity; x_m is the position of the mth element, while (x_f, z_f) refers to the phase center position of the feeder; and $(-1)^{B_m}$ denotes the reflection coefficient of element m. The diode switches between '0' and '1' states, corresponding to phase responses of 0° and 180°. In the "0" state, B_m is set to 0, resulting in a normalized reflection phase of 0°, which gives the element a reflection coefficient of 1. However, in the "1" state, the reflection coefficient is -1, corresponding to a phase response of 180°. The reflection amplitudes are assumed to be identical with the two states. In typical applications, the mutual influences of different signals are negligible. Hence, the received signal strength of a cell metasurface is

$$E\left[x(t_i)\, x(t_i)^*\right] = \sum_{n=1}^{N} R_n \left|F_E(\theta_n)\right|^2, \quad (2)$$

where $F_E(\theta)$ represents the far-field radiation pattern at angle θ, and R_n denotes the power level of the n^{th} signal. Assuming that the direction of arrival during a short sensing time is approximately constant, the incident signal is measured by generating L types of code matrix B. The received power matrix of the horn antenna for L sampling of the signal received could be defined as:

$$\mathbf{Y} = \mathbf{H}\mathbf{R}_S + \mathbf{n}, \quad (3)$$

$$\begin{bmatrix} y_1 \\ y_2 \\ \vdots \\ y_L \end{bmatrix} = \begin{bmatrix} H_1(\theta_1) & H_1(\theta_2) & \cdots & H_1(\theta_N) \\ H_2(\theta_1) & H_2(\theta_2) & \cdots & H_2(\theta_N) \\ \vdots & \vdots & \ddots & \vdots \\ H_L(\theta_1) & H_L(\theta_2) & \cdots & H_L(\theta_N) \end{bmatrix} \begin{bmatrix} R_{S1} \\ R_{S2} \\ \vdots \\ R_{SN} \end{bmatrix} + \begin{bmatrix} \sigma_1^2 \\ \sigma_2^2 \\ \vdots \\ \sigma_L^2 \end{bmatrix}, \quad (4)$$

where $R_S \in R^{N\times 1}$ denotes the incident signals source power; $Y = [y_1, y_2, \cdots, y_L]^t \in R^{L\times 1}$ represents the overall received power; and $H(\theta)$ represents the far-field radiation distribution corresponding to a particular coding configuration.

As shown in Figure 1(b), it is possible to divide the whole space equally into K parts, where $K \gg N$. Thus, the N incident signals are distributed sparsely. Thus, $\Theta = \left[\hat{\theta}_1, \hat{\theta}_2, \cdots, \hat{\theta}_N\right]^t$ can be solved using CS techniques

$$\begin{bmatrix} y_1 \\ y_2 \\ \vdots \\ y_L \end{bmatrix} = \begin{bmatrix} H_1(\theta_1) & H_1(\theta_2) & \cdots & H_1(\theta_K) \\ H_2(\theta_1) & H_2(\theta_2) & \cdots & H_2(\theta_K) \\ \vdots & \vdots & \ddots & \vdots \\ H_L(\theta_1) & H_L(\theta_2) & \cdots & H_L(\theta_K) \end{bmatrix} \begin{bmatrix} R_{S1} \\ R_{S2} \\ \vdots \\ R_{SK} \end{bmatrix} + \begin{bmatrix} \sigma_1^2 \\ \sigma_2^2 \\ \vdots \\ \sigma_L^2 \end{bmatrix}, \quad (5)$$

where $R_S \in R^{K\times 1}$, N elements are nonzero, and the values of K-N elements are zero. In addition, H denotes the measurement matrix based on compressed sensing (CS) theory, which can be solved using the $l1$-norm method or OMP algorithm. The DOA information can be obtained from the index of nonzero elements R_S.

The measurement matrix is an important parameter that directly affects the performance of DOA estimation. According to the MIP (Mutual Incoherence Properties) theory of compressive sensing, the reconstruction performance can be improved by reducing the correlation coefficient within the sensing matrix [48]. A programmable metasurface can generate entirely random radiation patterns to improve the orthogonality of the sensing matrix; nevertheless, it is more susceptible to discretization errors, such as those in the metasurface manufacturing process. Wang et al. [49] introduced the application of a random dual-beam radiation pattern instead of a completely physical random radiation pattern to generate a measurement matrix. Each dual-beam arrangement featured two primary lobes oriented in different random directions, and collectively, all dual-beam patterns encompassed the full space.

As shown in Figure 2(a), a reflective digital programmable metasurface (DPM) with 400 elements (20×20) was constructed, and DPM was configured using 40 coding schemes in order to sample the incident electromagnetic wave 40 different times. The whole sampled data create an observation vector, and the correlation coefficient of the measurement matrix is established. Figures 2(b)–(d) show the details of the unit cell, coding schemes, and far-field pattern, respectively. As demonstrated in Figure 2(e), the columns of the measurement matrix show low correlation coefficients. Figure 2(f) presents the spatial distribution of the radiation field associated with the 40 groups of aperture codes. The OMP algorithm was used to estimate DOA. In practice, the number of samples used by the OMP algorithm to estimate the angle of incidence for single and dual sources when the angle range is $-60°$ to $60°$ is 40, with an evaluation error under $1°$, as shown in Figures 2(g)–(l).

2.2. DOA Estimation Based on Space-Time-Coding Metasurfaces

The digital metasurface described in Subsection 2.1 is limited to encoding the spatial dimension, which regulates the scattering or radiation characteristics of EM waves in the near and far fields in the spatial domain [50–53]. The space-time metasurface introduces digital time-coded modulation into the space-coded metasurface and controls the change laws of the characterizing parameters of the metasurface in the spatial and temporal domains through joint coding of space and time dimensions, which can more accurately control the spatial and energy spectrum of EM waves [54, 55] and has greater degrees of freedom for real-time modulation of EM waves signals.

Figure 3 shows the concept of the modulation of EM waves by spatiotemporally coded digital metasurfaces [56]. Each cell in the space-time coded metasurface is loaded with switching diodes and controlled using the driving voltage provided by an FPGA digital module. Under different control voltages, the reflection coefficient of each cell dynamically changes according to the discrete phase or amplitude.

When the metasurface is switched in accordance with the designed space-time-coding matrix, the reflected EM waves illuminating the metasurface are manipulated in both the spatial and frequency domains. That is, the space-time-coding metasurface can not only control the spatial direction of reflected EM waves (spatial spectrum) but also control their harmonic energy distribution (frequency spectrum).

Thus, the scattering patterns on the metasurface of the space-time-coding can be controlled over different spectral types, such as fundamental and arbitrary harmonic frequencies. For an EM wave signal of $E_i = e^{j2\pi ft}$ with two-dimensional (2D) incident angles of (θ_i, φ_i), the far-field scattering pattern of the metasurface consisting of $N \times N$ individually addressable meta-atoms can be represented as follows:

$$f(\theta,\varphi,t) = \sum_{n=1}^{N}\sum_{m=1}^{N} E_{nm}(\theta,\varphi)\,\Gamma_{nm}(t)\times e^{j\frac{2\pi f}{c}[(m-1)(\sin\theta\cos\varphi+\sin\theta_i\cos\varphi_i)d_x+(m-1)(\sin\theta\cos\varphi+\sin\theta_i\cos\varphi_i)d_x]}, \quad (6)$$

where (θ, φ) represents the angle of the receiving antenna; $E_{nm}(\theta, \varphi)$ denotes the far-field pattern of the meta-atom located in the n^{th} row and m^{th} column; $\Gamma_{nm}(t)$ is the time-coding control signal applied to the respective meta-atom; and d_x and d_y indicate the distances between adjacent meta-atoms along the x- and y-axes, respectively.

The received signals at different sampling times are arranged as follows:

$$\begin{bmatrix} f(\theta,\varphi,t) \\ f(\theta,\varphi,t+T_0) \\ \vdots \\ f\left(\theta,\varphi,t+\left(N^2-1\right)T_0\right) \end{bmatrix} = \tilde{\mathbf{\Gamma}}\mathbf{A} = \begin{bmatrix} \Gamma_1^0 & \Gamma_2^0 & \cdots & \Gamma_{N^2}^0 \\ \Gamma_1^{T_0} & \Gamma_2^{T_0} & \cdots & \Gamma_{N^2}^{T_0} \\ \vdots & \vdots & \ddots & \vdots \\ \Gamma_1^{(N^2-1)T_0} & \Gamma_2^{(N^2-1)T_0} & \cdots & \Gamma_{N^2}^{(N^2-1)T_0} \end{bmatrix}$$

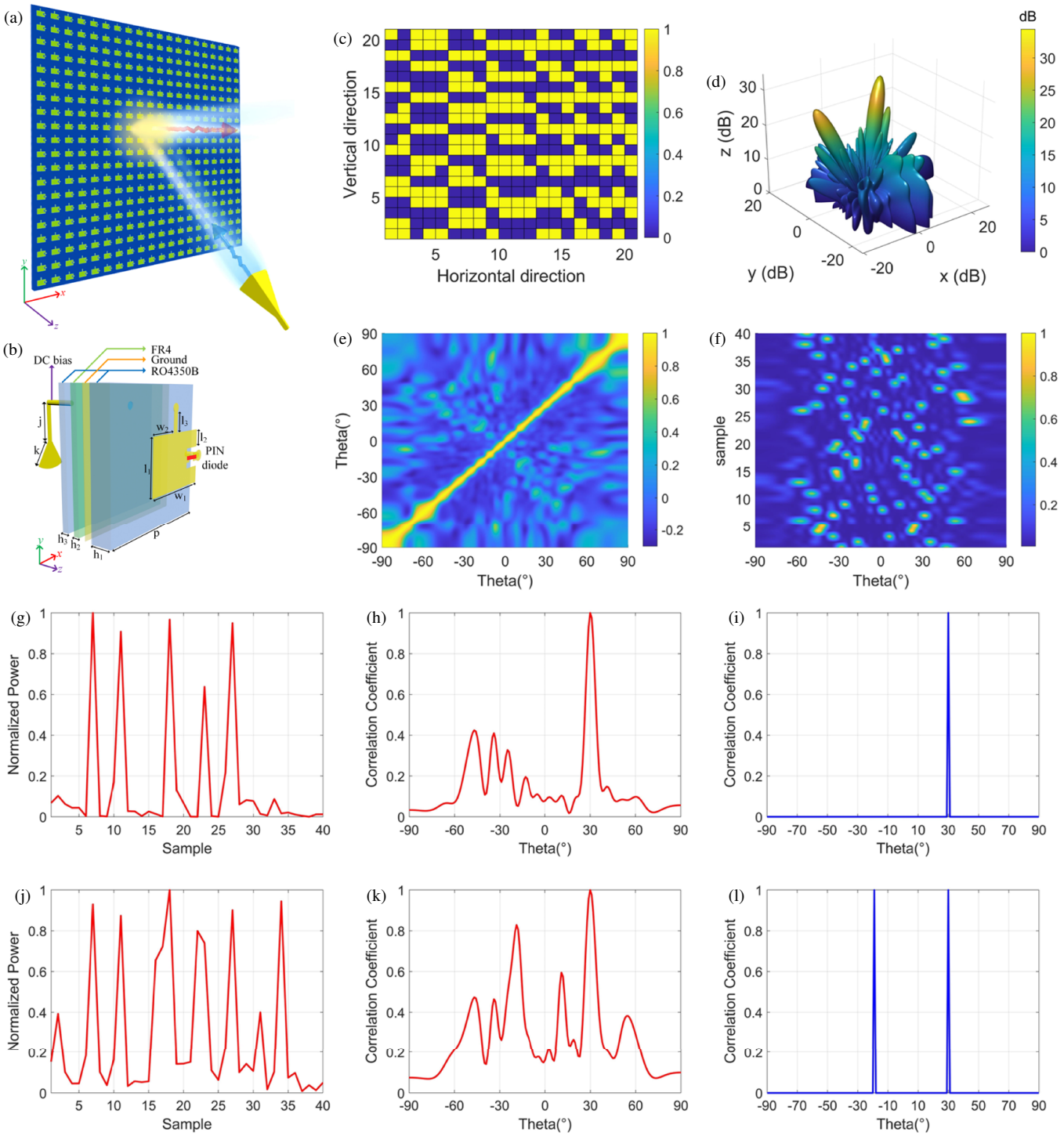

FIGURE 2. Concept and simulations of DOA estimations. (a) Mathematical model for DOA estimations via DPM. (b) Details of the unit cell. (c) Digital coding schemes for dual beams, with beams directed at $\theta_1 = 30^\circ$ and $\theta_2 = 10^\circ$. (d) Computed three-dimensional far-field pattern. (e) Correlation coefficients of the sensing matrix. (f) Radiation patterns [49]. (g), (j) Sampling energy in cases for the single-incidence and dual-incidence source cases, respectively. (h), (k) Estimated DOA for single-incidence and dual-incidence sources by projection method, respectively. (i), (l) DOA for single-incidence and dual-incidence sources estimated by the OMP algorithm, respectively [49]. Figures reproduced from: Ref. [49], Copyright 2021, John Wiley and Son.

$$\begin{bmatrix} A_1 \\ A_2 \\ \vdots \\ A_{N^2} \end{bmatrix} + \begin{bmatrix} \sigma_1^2 \\ \sigma_2^2 \\ \vdots \\ \sigma_{N^2}^2 \end{bmatrix} \tag{7}$$

where $\tilde{\Gamma}$ is a Hadamard matrix, and each row consists of N^2 unit-cells at a given sampling time. The signal vector $\mathbf{A}$ is collected from the incoming signals, and at the same time, the amplitude and phase distribution of the incident electromagnetic wave on the metasurface can also be reconstructed by it, i.e.,

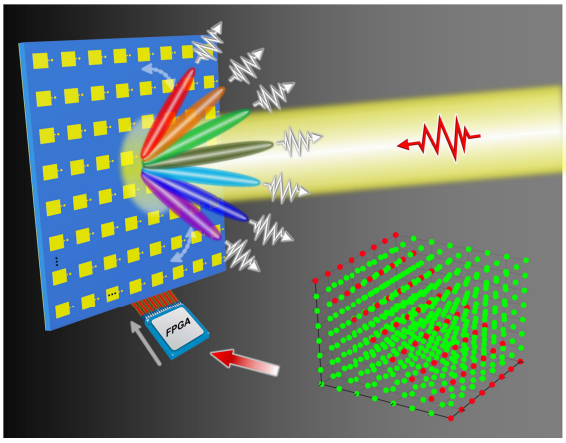

FIGURE 3. Conceptual depiction of a space-time-coding digital metasurface. Different control voltages can adjust the state of the PIN diode, and the reflection coefficient of the metasurface element can be dynamically adjusted using discrete phase or amplitude states [43]. Figures reproduced from: Ref. [43], Copyright 2024, Springer Nature.

wavefront shaping is realized. Subsequently, the incident angle can be estimated according to a conventional DOA mathematical model such as MUSIC.

To verify the proposed DOA estimation method, Zhou et al. [57] designed a 7×7 meta-atom, as shown in Figure 4(a). The unit cells are independently addressable and operate within the frequency range of 4.3–4.8 GHz providing a 1-bit phase shift in reflection. The top layer of the unit features two reflective patches (center symmetric), with a PIN diode mounted in the gap between them.

Figure 4(b) shows the simulation results of the amplitude in the frequency range of 4.3–4.8 GHz, with the phase difference stable at approximately 180°. Due to the manufacturing tolerance of the PIN diode, the simulation results deviate from the actual measurement results; however, the overall deviation is within 3° in the 2D space, as shown in Figures 4(c)–(e); the obtained results are acceptable for practical applications.

Figure 5 illustrates a comparison of the effects of the signal-to-noise ratio (SNR) on the DOA estimation performance of beam scanning (BS) and CS for various numbers of metasurface elements and sampling lengths [47]. Figure 5(a) illustrates the estimation accuracy versus SNR for different numbers of elements in the one-dimensional (1D) metasurface antenna, and Figure 5(b) shows the estimation accuracy for different sampling lengths. The DOA estimation accuracy significantly decreases at low SNRs.

In 2022, Xia et al. [58] proposed a nonuniform time modulation active metasurface based on an amplifier cascade, as shown in Figure 6. Amplifier device can lower the noise factor (F) of metasurface, enhance signal quality, and increase the accuracy of DOA estimation. This design provides a significant improvement in SNR compared to a conventional PIN diode because amplifier gain offsets the insertion loss between the metasurface and horn antenna. Importantly, the achieved noise figure (NF) is lower than that of other active devices, enhancing overall performance. However, harmonic nonlinear effects can be realized by amplifier-based metasurfaces, which not only increase the power density of harmonics, but also further improve signal quality.

As a result, a method based on harmonic analysis can yield high-performance DOA estimations [59]. As shown in Figure 6, an active metasurface comprising 5×5 elements is designed and simulated. The amplifier with a maximum gain of 9.8 dB is cascaded with the bias control circuit and integrated between the receiver and transmitter chips. The forward transmission coefficient at the central frequency is 8.5 dB. From the experimental results, it is obvious that the recommended method works well. The tunable metasurface enhances the incident wave power, which not only improves the signal quality but also enables highly accurate DOA estimation.

In recent years, time-modulated linear arrays have garnered increasing attention because of their simple structure [60–62]. The harmonic characteristic matrix (HCM) generated by periodic modulation changes with the incidence direction of the radio frequency (RF) signal, and the incidence angle is calculated by solving a linear equation system that includes HCM and the frequency spectrum of the received signal [63–65]. In 2022, Fang et al. [66] introduced a low-complexity method for DOA estimation utilizing double-sideband space-time modulated metasurfaces. As highlighted in Figure 7, the metasurface is used to generate the $\pm 1^{\text{st}}$ double-sideband harmonics with equal amplitude. By introducing the array delay, the scattering pattern of the $\pm 1^{\text{st}}$ harmonics is asymmetric, and the spatial modulation of target harmonics is realized. In the case of different incidence angles, the DOA estimation is realized based on different $\pm 1^{\text{st}}$ harmonic relationships received by the antenna placed in the far field with the vertical array, which can be stated as follows:

$$\theta_{\text{DOA}} = \sin^{-1}\left(\frac{2}{k_0 D}\tan^{-1}\left(\frac{|\text{AF}_1| - |\text{AF}_{-1}|}{|\text{AF}_1| + |\text{AF}_{-1}|}\frac{\cos\left(\pi\Delta\tilde{t}\right)}{\sin\left(\pi\Delta\tilde{t}\right)}\right)\right), \tag{8}$$

where $|\text{AF}_1|$ and $|\text{AF}_{-1}|$ are the $\pm 1^{\text{st}}$ harmonic amplitude values and $\Delta\tilde{t} = \Delta t/T_p$. This method simplifies the computational and hardware complexity; in addition, it can be extended to 2D direction finding. However, time delay errors compromise the accuracy of the estimation.

In 2023, Bai et al. [67] estimated the angles (azimuth and elevation) of a received signal through examination of the ratio between fundamental and harmonic components of the incident signal. In this method, the metasurface composed of $M \times N$ elements is separated into two subarrays based on the odd and even rows or columns, and the phase centers of the subarrays have a spacing of $\lambda/2$. The ratio of the fundamental modulation to the harmonic component of the incident signal can be calculated using the phase shift of the metasurface element.

The ratio of the first harmonic component to the fundamental component varies in the transverse modulation stage as follows

$$\beta_1 = \frac{\text{AF}(\theta, \varphi, 1)}{\text{AF}(\theta, \varphi, 0)} = -\frac{2(j+1)}{\pi}\tan\left(\frac{\pi D}{\lambda}\sin\theta\cos\varphi\right). \tag{9}$$

Similarly, in the longitudinal modulation phase, the ratio of the proportion of the first harmonic component relative to the

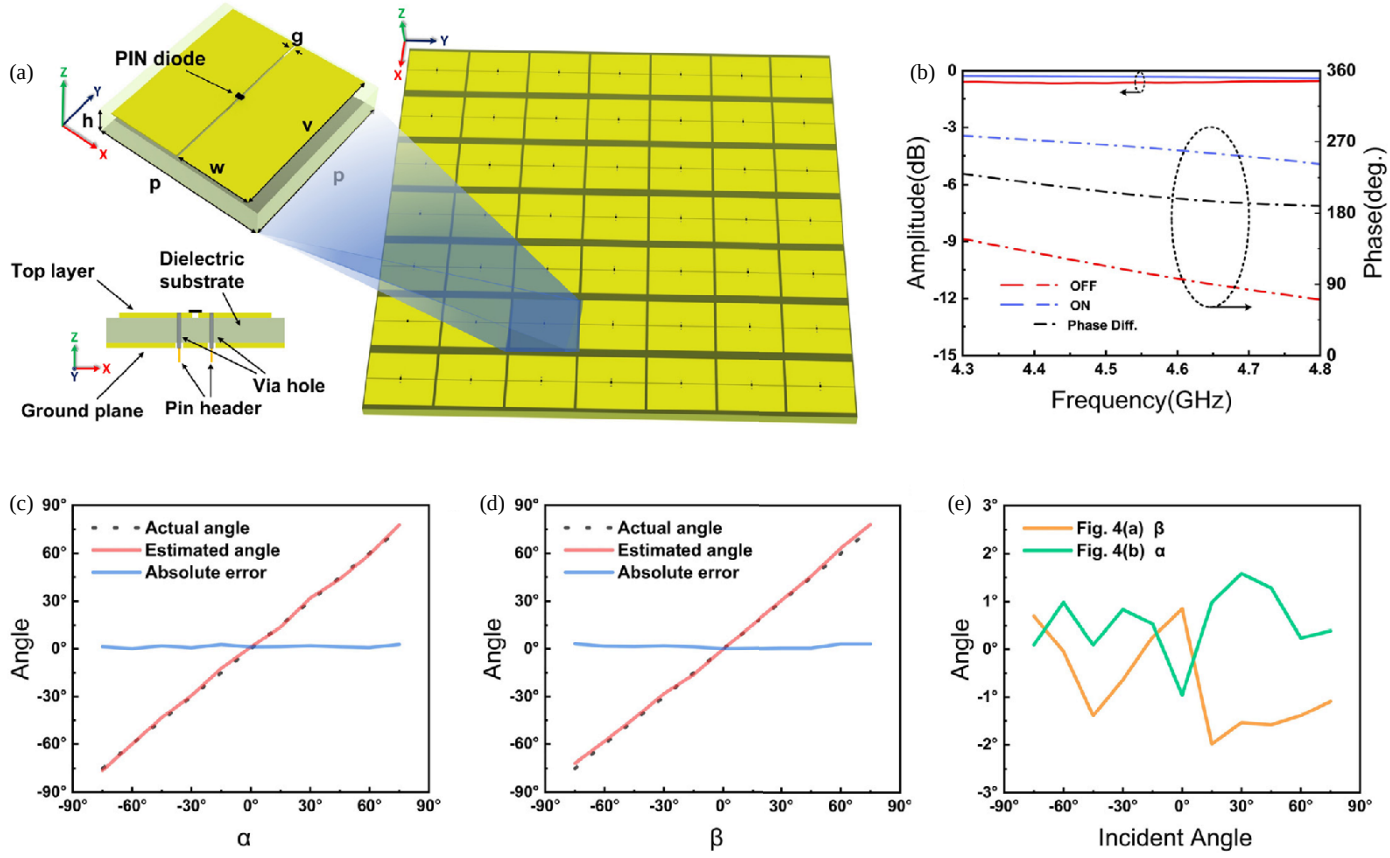

FIGURE 4. (a) Schematic of the metasurface. (b) Simulated reflection coefficients of the unit cell for the x-polarized incident wave, with the PIN diode in both ON and OFF states. (c) Actual angles, estimated angles, and absolute deviations when β is fixed at 0°. (d) Actual/estimated angles, and absolute deviations when α is set at 0°. (e) Estimated values of β in (c) and estimated α in (d) [57]. Figures reproduced from: Ref. [57], Copyright 2022, AIP Publishing.

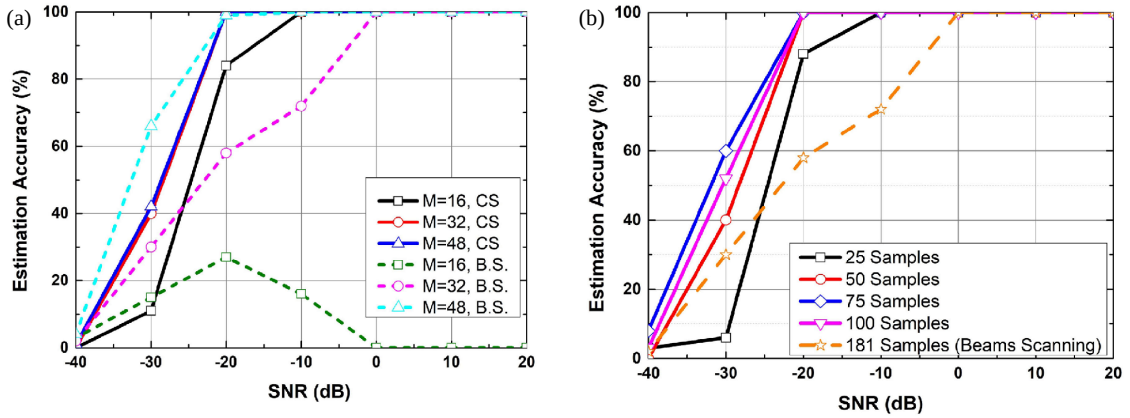

FIGURE 5. Estimation accuracy versus signal-to-noise ratio for different (a) metasurface antenna sizes and (b) sampling lengths [47]. Figures reproduced from: Ref. [47], Copyright 2021, IEEE.

fundamental component is calculated as follows:

$$\beta_2 = \frac{\mathrm{AF}(\theta,\varphi,1)}{\mathrm{AF}(\theta,\varphi,0)} = -\frac{2(j+1)}{\pi}\tan\left(\frac{\pi D}{\lambda}\sin\theta\sin\varphi\right). \quad (10)$$

Thus, the azimuth and elevation angles can be calculated to

$$\varphi_{est} = \begin{cases} \tan^{-1}\frac{\tan^{-1}(-\pi\beta_2/2(j+1))}{\tan^{-1}(-\pi\beta_1/2(j+1))}, & \sin\theta\cos\varphi > 0 \\ \pi + \tan^{-1}\frac{\tan^{-1}(-\pi\beta_2/2(j+1))}{\tan^{-1}(-\pi\beta_1/2(j+1))}, & \sin\theta\cos\varphi < 0 \end{cases}, \quad (11)$$

$$\theta_{est} = \sin^{-1}\frac{\lambda\tan^{-1}(-\pi\beta_2/2(j+1))}{2\pi D\sin\varphi_{est}}. \quad (12)$$

Figures 7(d)–(g) demonstrate the power spectrum of the metasurface-received signal at incidence angles of 0, +1, +2, and +3°. The mean square error (MSE) of the 14 direction findings was 0.21°. The estimated angles satisfactorily fit with the preset values, which demonstrates the accuracy of the proposed method. However, this method is significantly affected by SNR. When SNR reaches 20 dB, the trend of MSE of the

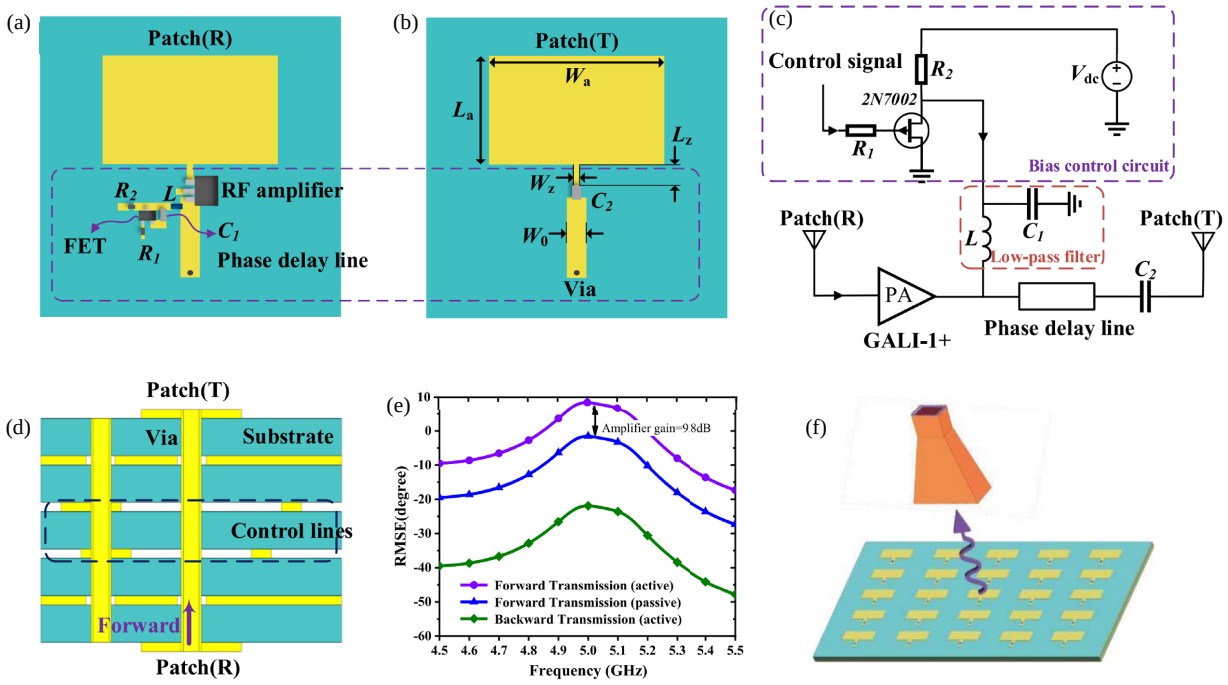

FIGURE 6. Active unit cell and metasurface aimed at boosting the incident wave. (a) and (b) Amplification and control circuits located on the top and bottom of the structure. (c) Diagram of the amplification and bias control circuits. (d) Side view of the stacked structure. (e) Simulation outcomes for the scattering parameters of the proposed element. (f) Active metasurface operating as a receiver [58]. Figures reproduced from: Ref. [58], Copyright 2022, John Wiley and Son.

direction finding is 0; however, the performance of the method sharply degrades when SNR decreases.

In 2019, by measuring and utilizing the delay information between different waveforms, Wang et al. [68] came up with a DOA estimation method based on spatial-temporal modulation meta-plane; this method achieved a 1D orientation, as illustrated in Figure 8.

As shown in Figure 8(a), an incoming wave $S(t)$ is incident on the space-time modulated metasurface with the angle θ (point (A) in Figure 8(a)), and the signal is transmitted to the receiving antenna (point (B) in Figure 8(a)) through the metasurface. This phenomenon is expressed as follows:

$$\begin{aligned} S_r(t) &= \sum_{m=1}^{N} m_k(t) S_k(t) \\ &= \sum_{m=1}^{N} m_k(t) S(t - t_0 - k\Delta\tau(\theta)), \end{aligned} \quad (13)$$

where t_0 is the time required for waves to travel in free space before encountering the metasurface; $m_k(t)$ is the kth orthogonal signal modulating code; $S_k(t)$ is a component of the incident wave that impinges on the k^{th} row of the metasurface; and $\Delta\tau(\theta)$ denotes the time difference between two neighboring rows, which is associated with the DOA angle-based array factor theory as follows:

$$\Delta\tau(\theta) = p\sin(\theta/c), \quad (14)$$

where p denotes the separation between two neighboring rows of the metasurface, while c represents the speed of light in free space. After orthogonality demodulation, the following expression is obtained:

$$S_k(t) = S(t - t_0 - k\Delta\tau(\theta)), \quad k = 1, 2, \cdots, N. \quad (15)$$

The waveforms $S_k(t)$ form an array of delayed replica of the signal that interacts with the metasurface, with a delay of $k\Delta\tau(\theta)$. As demonstrated in Figures 8(b) and (c), when the delay generated between adjacent waveforms is $\Delta\tau(\theta)$, DOA can be expressed as follows:

$$\theta_{\text{DOA}} = \sin^{-1}(c\Delta\tau/p). \quad (16)$$

Space-time modulated metasurfaces offer a more comprehensive approach by controlling both the spatial and frequency domains simultaneously. This dual modulation allows for precise manipulation of the wave's direction and spectral content, resulting in higher accuracy and robustness in DOA estimation. The ability to dynamically adjust both spatial and temporal parameters provides greater flexibility and can mitigate some of the issues faced by time-modulated metasurfaces in noisy environments. However, the increased complexity of space-time modulation may require more sophisticated control and processing systems.

On the other hand, time-modulated metasurfaces primarily affect DOA estimates by enhancing the frequency domain characteristics of the reflected waves. They introduce harmonic components that can be analyzed to determine the angle of arrival. This approach simplifies the computational complexity and can improve the accuracy of DOA estimation, especially in scenarios where frequency analysis is feasible. However, time-modulated metasurfaces may face challenges in low SNR

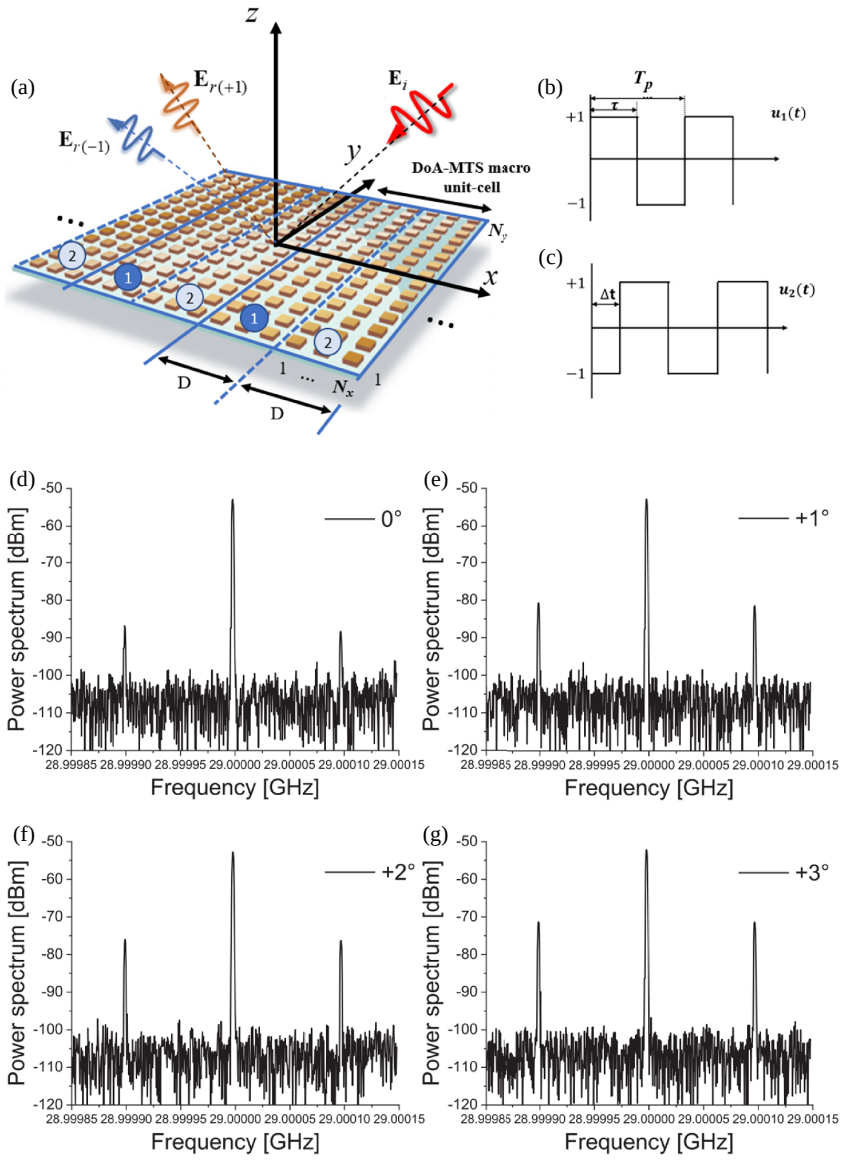

FIGURE 7. (a) Schematic of the space-time modulation scheme implemented for DOA estimation. (b) and (c) Temporal signals utilized to modulate two sub-microcells within the DOA-MTS macro unit-cell [66]. (d)–(g) Power spectra of received signals from various directions. (d) 0°, (e) +1°, (f) +2°, and (g) +3° [67]. Figures reproduced from: (a)–(c) Ref. [66], Copyright 2022, IEEE. (d)–(g) Ref. [67], Copyright 2023, IEEE.

environments, as noise can significantly impact the harmonic analysis.

Recently, integration of artificial intelligence algorithms (such as machine learning, deep learning) and metasurfaces has garnered widespread attention in various applications. In addition, DOA estimation using machine learning-enabled metasurfaces has been proposed. Chen et al. [69] combined an artificial neural network with a space-time-coding digital metasurface and proposed neural network models with multiple training strategies using only phase-free normalized harmonic amplitude. After training the measured data, a high estimation accuracy was achieved. Huang et al. [11] used a reconfigurable metasurface for transmission wave operation and adopted deep neural network (DNN) algorithm as an intelligent calculation to avoid a large amount of data processing; the DOA estimation error reached 0.5°. The proposed method based on artificial intelligence has a simple hardware structure, requires small number of calculations, and reasonable robustness and practicability. However, large amounts of training data are required to obtain high-precision DOA estimations.

2.3. DOA Estimation Based on Lens Metasurface

Compared to phased-array antennas, multibeam lenses have the characteristics of low cost, wide frequency band, wide angular scanning, and simple structure [9]. Multibeam lenses provide an extremely attractive solution in the fields of satellite navigation, high-rate communication, and military electronics. The use of a metasurface technology to control EM parameters of the lens material can reduce processing difficulty and production cost, making the lens more advantageous for engineering applications.

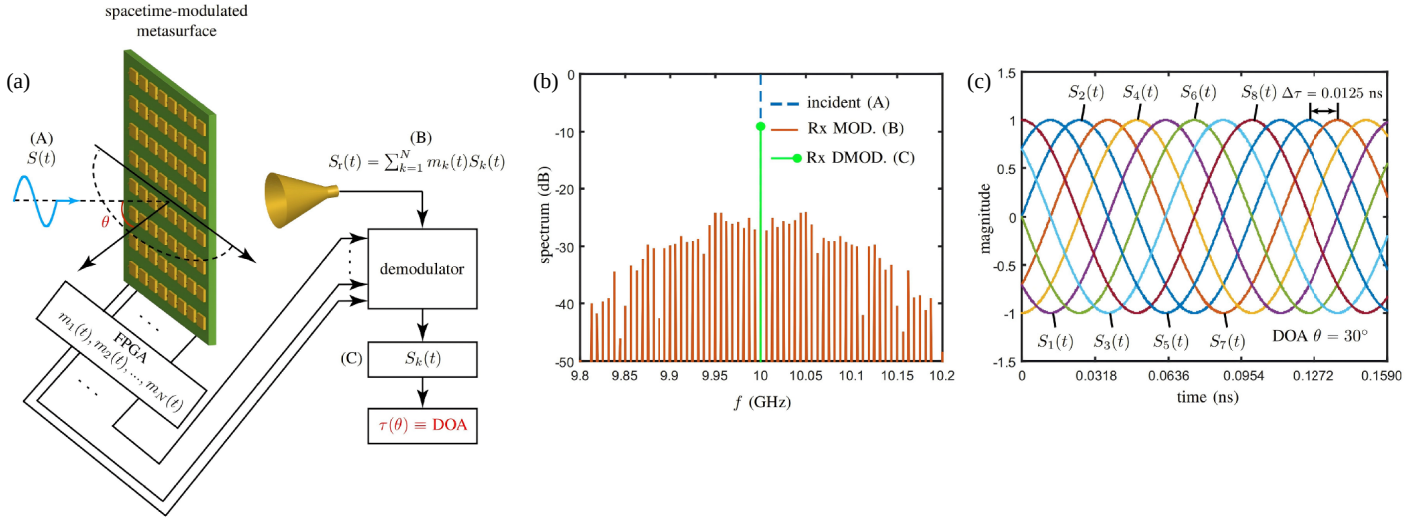

FIGURE 8. Concept of DOA estimation based on a spacetime-modulated and simulation results [68]. (a) Concept of DOA estimation. (b) Spectra of the incident signal, the received signal before and after demodulation. (c) Signal waveform (after demodulation). Figures reproduced from: Ref. [68], Copyright 2019, IEEE.

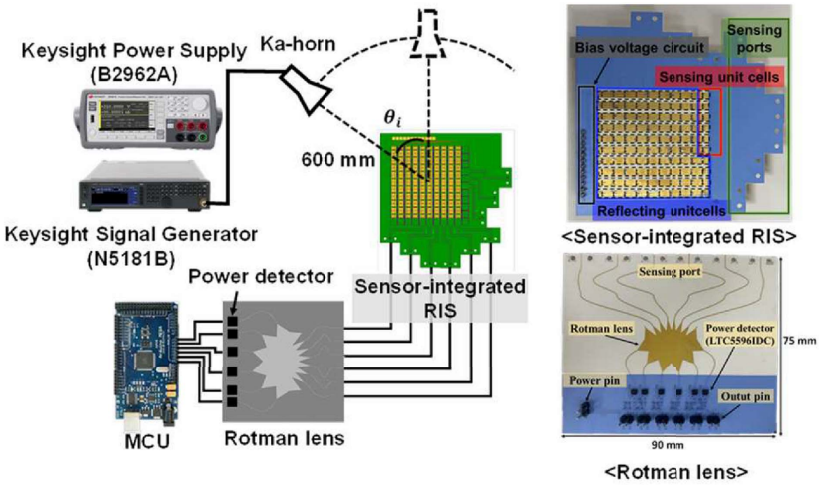

FIGURE 9. Rotman lens sensing measurement device and related structures [50]. Figures reproduced from: Ref. [50], Copyright 2023, IEEE.

The multibeam antenna system based on the Rotman lens has the characteristics [70] of all-round interception probability, high direction-finding accuracy, large dynamic range, and high sensitivity, making it appropriate for the use on platforms with high volume, weight, power consumption, and cost requirements [71]. In 2023, Hwang et al. [72] integrated a reconfigurable intelligent surface (RIS) unit with a Rotman lens to implement real-time DOA estimation and adaptive beamforming using a simple RF link and microcontroller unit (MCU). As shown in Figure 9, the designed sensing system consists of an RIS, a Rotman lens, an RF power detector, and an MCU. RIS includes 10×10 cells, of which 94 unit-cell functions are used as reflection units (beamforming), and six unit-cell functions serve as sensing units (DOA estimation). Six sensing cells are strategically positioned at the edges of the RIS to connect to the Rotman lens, ensuring minimal insertion loss. A power detector is connected to the output port of the Rotman lens, allowing for precise measurement of power levels across all ports. The angle of incidence is determined by comparing the measured value to a code that identifies the port with the highest and second highest voltage levels based on previous simulations. The position of the emitter can be estimated from the angle, e.g., calculated in 15° increments over the range $-45°$ to 45°. Additionally, increasing the number of ports in the Rotman lens would enable a wider sensing range while enhancing angular resolution, making it possible to accurately track signals across a broader spectrum of angles. This approach not only improves performance but also provides greater flexibility in applications requiring precise directional measurements.

According to the estimated value of DOA, the system controls the reflection unit through Pulse Width Modulation (PWM), applies the corresponding bias voltage to the PIN diode, and controls the reflected signal to transmit a signal beam to the desired point. This simple structure, low-cost DOA sensing, and adaptive beamforming system are appropriate for 5G communication applications.

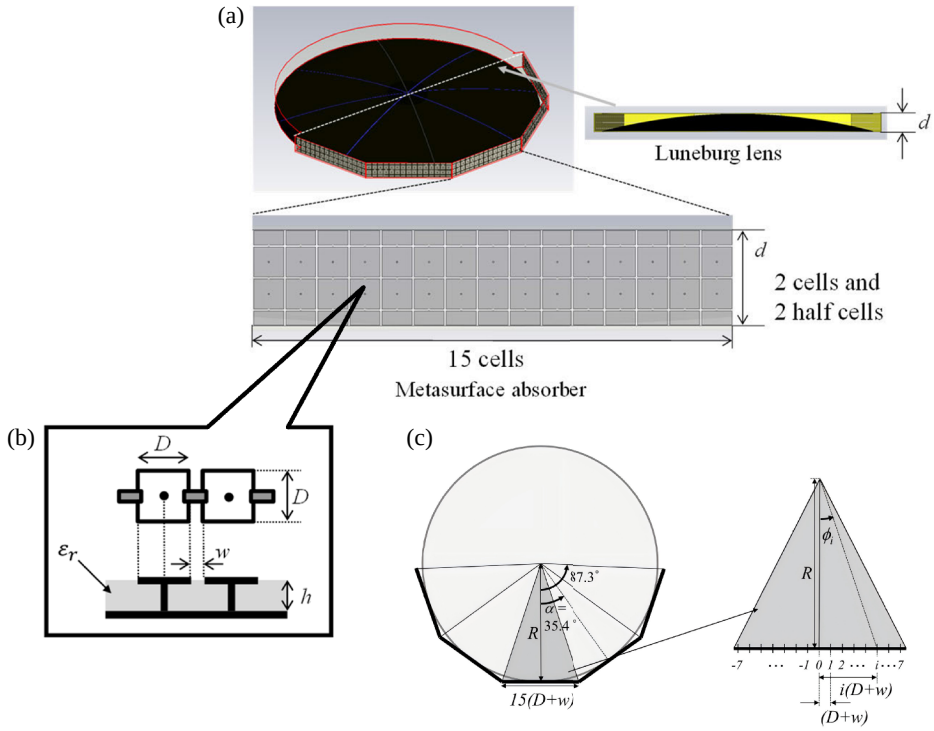

FIGURE 10. (a) Framework for DOA estimation involving a planar Luneburg lens and a metasurface absorber. (b) Absorber utilizing a waveguide metasurface. (c) Position and detection angle of metasurface absorber [73]. Figures reproduced from: Ref. [73], Copyright 2023, IEEE.

A Luneburg lens is a dielectric lens with a graded refractive index that yields BS and multibeam focusing by converging an incident wave of a specific frequency to a certain point on the lens surface. In 2023, Ohmae and Yagitani [73] proposed a unique DOA estimation method, which utilizes a planar Luneburg lens in combination with a waveguide metasurface absorber to achieve a system compactness effect. Figure 10 shows this lens.

A series of two-dimensional square patch arrays form a metasurface absorber. The metasurface absorber and each patch have a metal through-hole at the center for connection to a ground plane. As illustrated in Figure 10(b), d is the distance between the parallel plates (waveguide); D represents the size of patches; ε_r denotes the relative permittivity of the dielectric material; h indicates the substrate thickness; w is the gap between patches. This configuration enhances the absorption characteristics and allows for effective energy dissipation in the metasurface design. Figure 10(a) shows the overall structure of the proposed system. The five printed circuit boards are arranged around the lens to form the metasurface absorber. The receiving planes on each printed circuit board (PCB) are placed as close as possible to the focal point of the lens. The lens and PCB can be completely encapsulated by the upper and lower waveguides. Each PCB features a metasurface absorber consisting of two vertical cells and two half-cells, along with 15 horizontal cells, as depicted in Figure 10(b). This arrangement maximizes the absorber's effectiveness by optimizing the interaction between the incoming waves and designed structure, enhancing overall performance. Fifteen sensor cells are evenly spaced horizontally for $D + w$. The angle of the ith receiving sensor can be obtained as follows:

$$\varphi_i = \tan^{-1} \frac{i\,(D+w)}{R}. \tag{17}$$

As shown in Figure 10(c), $D = 8.0\,\text{mm}$, $w = 0.5\,\text{mm}$, $R = 200\,\text{mm}$, detection points are placed every 8.5 mm; the furthest detection position is $\pm 59.5\,\text{mm}$; the central PCB can detect an angle of $\pm 16.6°$; the interval between adjacent boards is 35.4°; and the detectable angle by the system is $\pm 87.3°$. The experimental results show that the maximum error of the DOA estimation in the frequency band of 5.65 GHz is 2.4°.

DOA systems based on lenses and metasurfaces have the benefits of compact structure, convenient measurement, and high direction-finding accuracy without complicated calculations. Therefore, these systems have broad application prospects in both military and civilian fields.

3. CONCLUSION

This paper has provided an extensive review of the current research on Direction of Arrival (DOA) estimation technologies leveraging programmable metasurfaces. We have examined three primary types of metasurfaces utilized for DOA estimation: digital coding metasurfaces, space-time-coding metasurfaces, and lens metasurfaces. Each type offers unique advantages and demonstrates the potential of metasurfaces to revolutionize DOA estimation.

Digital coding metasurfaces have been shown to simplify the sensing process by requiring only a single radio frequency receiving channel, which reduces the complexity and cost of the

system while maintaining high-resolution capabilities through the use of Orthogonal Matching Pursuit (OMP) and other sparse recovery algorithms. The tunable nature of these metasurfaces allows for dynamic manipulation of electromagnetic waves, offering a flexible and adaptable platform for DOA estimation.

Space-time-coding metasurfaces extend the capabilities of digital coding metasurfaces by introducing time modulation into the spatial domain. This dual-dimensional control over electromagnetic waves provides greater degrees of freedom for real-time modulation, enhancing the accuracy and flexibility of DOA estimation further. The integration of artificial intelligence algorithms with these metasurfaces has shown promising results, offering high estimation accuracy with reduced computational complexity.

Lens metasurfaces, including Rotman lens and Luneburg lens systems, offer a compact and cost-effective solution for DOA estimation. By combining the advantages of lens technology with the tunable properties of metasurfaces, these systems achieve high direction-finding accuracy with simplified measurement processes. The integration of sensors with the lens for real-time DOA estimation and adaptive beamforming demonstrates the potential for practical applications in 5G and beyond.

The potential impact of metasurfaces on broader applications, such as 6G and next-generation satellite communications, is significant. Metasurfaces offer a pathway to overcome the limitations of traditional antenna systems by providing reconfigurable, compact, and low-profile solutions. Their ability to manipulate electromagnetic waves with precision can lead to improved signal quality, enhanced communication links, and the enablement of new functionalities in wireless communication systems. In 6G, metasurfaces are expected to play a crucial role in the development of smart surfaces and reconfigurable environments, which can adapt to different communication scenarios in real-time. For satellite communications, metasurfaces can contribute to the miniaturization of terminals, the enhancement of signal directivity, and the mitigation of signal interference, thereby improving the overall efficiency and reliability of the communication link.

DOA estimation has significant applications in numerous fields, including communication, radar, and military operations. Achieving high-precision DOA estimations traditionally necessitates a large number of antenna array units, which results in complex, large-scale receiving systems, intricate calculations, and high costs. This review has highlighted that reconfigurable metasurfaces offer advantages such as low cost, low energy consumption, and ease of deployment. These features make them suitable for integrating and miniaturizing DOA estimation systems, thus balancing accuracy and practicality. Despite the reliable results obtained from comprehensive studies, several challenges remain and must be addressed for practical applications and successful commercialization. One significant issue is that once the metasurface material and structure are set, the operating frequency is generally fixed, limiting the frequency range. Therefore, they are mostly suitable for applications requiring a fixed frequency or limited bandwidth. Expanding their applicability across multiple octaves requires further advancements. Moreover, the capability of DOA estimation is significantly influenced by the consistency of multiple metasurface elements. Hence, further research is necessary for optimizing the design and calibration of these elements to enhance the overall performance of DOA estimation systems. Addressing these challenges will pave the way for the practical implementation and broader adoption of metasurface-based DOA estimation technologies.

ACKNOWLEDGEMENT

The Key Research and Development Program of Zhejiang Province under Grant No. 2024C01160, the Postdoctoral Science Preferential Funding of Zhejiang Province under Grant No. ZJ2024055, and Postdoctoral Fellowship Program of CPSF under Grant No. GZB20230654.

REFERENCES

[1] Van Trees, H. L., *Detection, Estimation, and Modulation Theory, Optimum Array Processing*, 1472, John Wiley & Sons, 2004.

[2] Henault, S., S. Rajan, R. Inkol, S. Wang, and Y. M. M. Antar, "Impact of elevation angle variations in wideband adcock direction finders subject to mutual coupling," in *2008 IEEE Antennas and Propagation Society International Symposium*, 1–4, San Diego, CA, USA, 2008.

[3] Ly, P. Q. C., S. D. Elton, and D. A. Gray, "AOA estimation of two narrowband signals using interferometry," in *2010 IEEE International Symposium on Phased Array Systems and Technology*, 1004–1009, Waltham, MA, USA, 2010.

[4] Sai, J., C. Yao, and R. Chen, "Design of a single channel Doppler direction finding system," in *2021 International Conference on Neural Networks, Information and Communication Engineering*, Vol. 11933, 119332F, Qingdao, China, 2021.

[5] Zhou, C., Z. Shi, Y. Gu, and X. Shen, "DECOM: DOA estimation with combined MUSIC for coprime array," in *2013 International Conference on Wireless Communications and Signal Processing*, 1–5, Hangzhou, China, 2013.

[6] Li, J., D. Jiang, and X. Zhang, "DOA estimation based on combined unitary ESPRIT for coprime MIMO radar," *IEEE Communications Letters*, Vol. 21, No. 1, 96–99, 2017.

[7] Beking, M. V. T., "Sparse array antenna signal reconstruction using compressive sensing for direction of arrival estimation," M.Sc. Thesis, Faculty of Electrical Engineering, Mathematics and Computer Science, University of Twente, Enschede, Netherlands, 2016.

[8] Chen, D., L. Tian, and C. Xu, "MMV-based OMP for DOA estimation with 1-bit measurement," in *Journal of Physics: Conference Series*, Vol. 1550, No. 3, 032150, 2020.

[9] Liu, C., Y. V. Zakharov, and T. Chen, "Broadband underwater localization of multiple sources using basis pursuit de-noising," *IEEE Transactions on Signal Processing*, Vol. 60, No. 4, 1708–1717, 2012.

[10] Liang, M., X. Yu, R. Sabory-García, W.-R. Ng, M. E. Gehm, and H. Xin, "Direction of arrival estimation using Luneburg lens," in *2012 IEEE/MTT-S International Microwave Symposium Digest*, 1–3, Montreal, QC, Canada, Jun. 2012.

[11] Huang, M., B. Zheng, T. Cai, X. Li, J. Liu, C. Qian, and H. Chen, "Machine-learning-enabled metasurface for direction of arrival estimation," *Nanophotonics*, Vol. 11, No. 9, 2001–2010, 2022.

[12] Huang, M., B. Zheng, R. Li, X. Li, Y. Zou, T. Cai, and H. Chen, "Diffraction neural network for multi-source information of ar-

rival sensing," *Laser & Photonics Reviews*, Vol. 17, No. 10, 2300202, 2023.
[13] Ding, X., Z. Wang, G. Hu, J. Liu, K. Zhang, H. Li, B. Ratni, S. N. Burokur, Q. Wu, J. Tan, and C.-W. Qiu, "Metasurface holographic image projection based on mathematical properties of fourier transform," *PhotoniX*, Vol. 1, 1–12, 2020.
[14] Zou, Y., R. Zhu, L. Shen, and B. Zheng, "Reconfigurable metasurface hologram of dynamic distance via deep learning," *Frontiers in Materials*, Vol. 9, 907672, 2022.
[15] Yang, H., X. Cao, F. Yang, J. Gao, S. Xu, M. Li, X. Chen, Y. Zhao, Y. Zheng, and S. Li, "A programmable metasurface with dynamic polarization, scattering and focusing control," *Scientific Reports*, Vol. 6, No. 1, 1–11, 2016.
[16] Hu, Y., X. Liu, M. Jin, Y. Tang, X. Zhang, K. F. Li, Y. Zhao, G. Li, and J. Zhou, "Dielectric metasurface zone plate for the generation of focusing vortex beams," *PhotoniX*, Vol. 2, No. 1, 10, 2021.
[17] Lu, H., J. Zhao, B. Zheng, C. Qian, T. Cai, E. Li, and H. Chen, "Eye accommodation-inspired neuro-metasurface focusing," *Nature Communications*, Vol. 14, No. 1, 3301, 2023.
[18] Zhao, Z., Y. Wang, C. Guan, K. Zhang, Q. Wu, H. Li, J. Liu, S. N. Burokur, and X. Ding, "Deep learning-enabled compact optical trigonometric operator with metasurface," *PhotoniX*, Vol. 3, No. 1, 15, 2022.
[19] Zheng, X., J. Lin, Z. Wang, H. Zhou, Q. He, and L. Zhou, "Manipulating light transmission and absorption via an achromatic reflectionless metasurface," *PhotoniX*, Vol. 4, No. 1, 3, 2023.
[20] Jia, Y., C. Qian, Z. Fan, Y. Ding, Z. Wang, D. Wang, E.-P. Li, B. Zheng, T. Cai, and H. Chen, "In situ customized illusion enabled by global metasurface reconstruction," *Advanced Functional Materials*, Vol. 32, No. 19, 2109331, 2022.
[21] Sun, S., Q. He, J. Hao, S. Xiao, and L. Zhou, "Electromagnetic metasurfaces: Physics and applications," *Advances in Optics and Photonics*, Vol. 11, No. 2, 380–479, 2019.
[22] Liu, F., O. Tsilipakos, A. Pitilakis, A. C. Tasolamprou, M. S. Mirmoosa, N. V. Kantartzis, D.-H. Kwon, J. Georgiou, K. Kossifos, M. A. Antoniades, *et al.*, "Intelligent metasurfaces with continuously tunable local surface impedance for multiple reconfigurable functions," *Physical Review Applied*, Vol. 11, No. 4, 044024, 2019.
[23] Jung, M., W. Saad, M. Debbah, and C. S. Hong, "On the optimality of reconfigurable intelligent surfaces (RISs): Passive beamforming, modulation, and resource allocation," *IEEE Transactions on Wireless Communications*, Vol. 20, No. 7, 4347–4363, 2021.
[24] Zhu, R., D. Liu, H. Lu, L. Peng, T. Cai, and B. Zheng, "High-efficiency Pancharatnam-Berry metasurface-based surface plasma coupler," *Advanced Photonics Research*, Vol. 5, No. 2, 2300315, 2024.
[25] Bai, X., F. Zhang, L. Sun, A. Cao, C. He, J. Zhang, and W. Zhu, "Dynamic millimeter-wave OAM beam generation through programmable metasurface," *Nanophotonics*, Vol. 11, No. 7, 1389–1399, 2022.
[26] Chen, H., L. Ran, J. Huangfu, X. Zhang, K. Chen, T. M. Grzegorczyk, and J. A. Kong, "Left-handed materials composed of only S-shaped resonators," *Physical Review E*, Vol. 70, No. 5, 057605, 2004.
[27] Yang, Y., Z. Gao, H. Xue, L. Zhang, M. He, Z. Yang, R. Singh, Y. Chong, B. Zhang, and H. Chen, "Realization of a three-dimensional photonic topological insulator," *Nature*, Vol. 565, No. 7741, 622–626, 2019.
[28] Cai, T., B. Zheng, J. Lou, L. Shen, Y. Yang, S. Tang, E. Li, C. Qian, and H. Chen, "Experimental realization of a superdispersion-enabled ultrabroadband terahertz cloak," *Advanced Materials*, Vol. 34, No. 38, 2205053, 2022.
[29] Yang, Y., L. Jing, B. Zheng, R. Hao, W. Yin, E. Li, C. M. Soukoulis, and H. Chen, "Full-polarization 3D metasurface cloak with preserved amplitude and phase," *Advanced Materials*, Vol. 28, No. 32, 6866–6871, 2016.
[30] Li, Z., W. Liu, Y. Zhang, H. Cheng, S. Zhang, and S. Chen, "Optical polarization manipulations with anisotropic nanostructures," *PhotoniX*, Vol. 5, No. 1, 30, 2024.
[31] Hu, J., H. Zhang, B. Di, L. Li, K. Bian, L. Song, Y. Li, Z. Han, and H. V. Poor, "Reconfigurable intelligent surface based RF sensing: Design, optimization, and implementation," *IEEE Journal on Selected Areas in Communications*, Vol. 38, No. 11, 2700–2716, 2020.
[32] Alexandropoulos, G. C., N. Shlezinger, I. Alamzadeh, M. F. Imani, H. Zhang, and Y. C. Eldar, "Hybrid reconfigurable intelligent metasurfaces: Enabling simultaneous tunable reflections and sensing for 6G wireless communications," *IEEE Vehicular Technology Magazine*, Vol. 19, No. 1, 75–84, 2023.
[33] Zhao, J., Q. Yu, B. Qian, K. Yu, Y. Xu, H. Zhou, and X. Shen, "Fully-decoupled radio access networks: A resilient uplink base stations cooperative reception framework," *IEEE Transactions on Wireless Communications*, Vol. 22, No. 8, 5096–5110, 2023.
[34] Zheng, B., H. Lu, C. Qian, D. Ye, Y. Luo, and H. Chen, "Revealing the transformation invariance of full-parameter omnidirectional invisibility cloaks," *Electromagnetic Science*, Vol. 1, No. 2, 1–7, 2023.
[35] Chen, H., B.-I. Wu, B. Zhang, and J. A. Kong, "Electromagnetic wave interactions with a metamaterial cloak," *Physical Review Letters*, Vol. 99, No. 6, 063903, 2007.
[36] Qian, C., B. Zheng, Y. Shen, L. Jing, E. Li, L. Shen, and H. Chen, "Deep-learning-enabled self-adaptive microwave cloak without human intervention," *Nature Photonics*, Vol. 14, No. 6, 383–390, 2020.
[37] Huang, M., B. Zheng, R. Li, L. Shen, X. Li, H. Lu, R. Zhu, T. Cai, and H. Chen, "Evolutionary games-assisted synchronization metasurface for simultaneous multisource invisibility cloaking," *Advanced Functional Materials*, Vol. 34, No. 36, 2401909, 2024.
[38] Qian, C., Y. Jia, Z. Wang, J. Chen, P. Lin, X. Zhu, E. Li, and H. Chen, "Autonomous aeroamphibious invisibility cloak with stochastic-evolution learning," *Advanced Photonics*, Vol. 6, No. 1, 016001, 2024.
[39] Zhou, W., S. Zhu, Z. Zhang, R. Zhu, B. Chen, J. Zhao, X. Wei, H. Lu, and B. Zheng, "Time-varying metasurface driven broadband radar jamming and deceptions," *Optics Express*, Vol. 32, No. 10, 17 911–17 921, 2024.
[40] Qian, C., X. Lin, X. Lin, J. Xu, Y. Sun, E. Li, B. Zhang, and H. Chen, "Performing optical logic operations by a diffractive neural network," *Light: Science & Applications*, Vol. 9, No. 1, 59, 2020.
[41] Chen, H., B. Zheng, L. Shen, H. Wang, X. Zhang, N. I. Zheludev, and B. Zhang, "Ray-optics cloaking devices for large objects in incoherent natural light," *Nature Communications*, Vol. 4, No. 1, 1–6, 2013.
[42] Zhang, L., Y. Yang, Y. Ge, Y.-J. Guan, Q. Chen, Q. Yan, F. Chen, R. Xi, Y. Li, D. Jia, *et al.*, "Acoustic non-hermitian skin effect from twisted winding topology," *Nature Communications*, Vol. 12, No. 1, 6297, 2021.
[43] Xi, S., H. Chen, T. Jiang, L. Ran, J. Huangfu, B.-I. Wu, J. A. Kong, and M. Chen, "Experimental verification of reversed Cherenkov radiation in left-handed metamaterial," *Physical Review Letters*, Vol. 103, No. 19, 194801, 2009.

[44] Qian, C., X. Lin, Y. Yang, X. Xiong, H. Wang, E. Li, I. Kaminer, B. Zhang, and H. Chen, "Experimental observation of superscattering," *Physical Review Letters*, Vol. 122, No. 6, 063901, 2019.

[45] Hoang, T. V., R. Sharma, V. Fusco, and O. Yurduseven, "Single-pixel compressive direction of arrival estimation using programmable metasurface apertures," in *Passive and Active Millimeter-Wave Imaging XXIV*, Vol. 11745, 117450B, Apr. 2021.

[46] Wymeersch, H., J. He, B. Denis, A. Clemente, and M. Juntti, "Radio localization and mapping with reconfigurable intelligent surfaces: Challenges, opportunities, and research directions," *IEEE Vehicular Technology Magazine*, Vol. 15, No. 4, 52–61, 2020.

[47] Lin, M., M. Xu, X. Wan, H. Liu, Z. Wu, J. Liu, B. Deng, D. Guan, and S. Zha, "Single sensor to estimate DOA with programmable metasurface," *IEEE Internet of Things Journal*, Vol. 8, No. 12, 10 187–10 197, 2021.

[48] Hu, J., H. Zhang, K. Bian, M. D. Renzo, Z. Han, and L. Song, "MetaSensing: Intelligent metasurface assisted RF 3D sensing by deep reinforcement learning," *IEEE Journal on Selected Areas in Communications*, Vol. 39, No. 7, 2182–2197, 2021.

[49] Wang, J. W., Z. A. Huang, Q. Xiao, W. H. Li, B. Y. Li, X. Wan, and T. J. Cui, "High-precision direction-of-arrival estimations using digital programmable metasurface," *Advanced Intelligent Systems*, Vol. 4, No. 4, 2100164, 2022.

[50] Cui, T. J., M. Q. Qi, X. Wan, J. Zhao, and Q. Cheng, "Coding metamaterials, digital metamaterials and programmable metamaterials," *Light: Science & Applications*, Vol. 3, No. 10, e218, 2014.

[51] Wang, M., H. F. Ma, L. W. Wu, S. Sun, W. X. Tang, and T. J. Cui, "Hybrid digital coding metasurface for independent control of propagating surface and spatial waves," *Advanced Optical Materials*, Vol. 7, No. 13, 1900478, 2019.

[52] Cui, T. J., "Microwave metamaterials — From passive to digital and programmable controls of electromagnetic waves," *Journal of Optics*, Vol. 19, No. 8, 084004, 2017.

[53] Liu, S., L. Zhang, G. D. Bai, and T. J. Cui, "Flexible controls of broadband electromagnetic wavefronts with a mechanically programmable metamaterial," *Scientific Reports*, Vol. 9, No. 1, 1809, 2019.

[54] Dai, J. Y., W. Tang, M. Wang, M. Z. Chen, Q. Cheng, S. Jin, T. J. Cui, and C. H. Chan, "Simultaneous in situ direction finding and field manipulation based on space-time-coding digital metasurface," *IEEE Transactions on Antennas and Propagation*, Vol. 70, No. 6, 4774–4783, Jun. 2022.

[55] Ni, G., C. He, J. Chen, Y. Liu, X. Jiang, R. Jin, and L. Bai, "Array signal recovery and direction-finding based on non-uniform period modulation," in *2020 9th Asia-Pacific Conference on Antennas and Propagation (APCAP)*, 1–2, Xiamen, China, 2020.

[56] Zhang, L., X. Q. Chen, S. Liu, Q. Zhang, J. Zhao, J. Y. Dai, G. D. Bai, X. Wan, Q. Cheng, G. Castaldi, V. Galdi, and T. J. Cui, "Space-time-coding digital metasurfaces," *Nature Communications*, Vol. 9, No. 1, 4334, 2018.

[57] Zhou, Q. Y., J. W. Wu, S. R. Wang, Z. Q. Fang, L. J. Wu, J. C. Ke, J. Y. Dai, T. J. Cui, and Q. Cheng, "Two-dimensional direction-of-arrival estimation based on time-domain-coding digital metasurface," *Applied Physics Letters*, Vol. 121, No. 18, 181702, 2022.

[58] Xia, D., X. Wang, J. Han, H. Xue, G. Liu, Y. Shi, L. Li, and T. J. Cui, "Accurate 2-D DOA estimation based on active metasurface with nonuniformly periodic time modulation," *IEEE Transactions on Microwave Theory and Techniques*, Vol. 71, No. 8, 3424–3435, 2022.

[59] Wang, X., J. Han, S. Tian, D. Xia, L. Li, and T. J. Cui, "Amplification and manipulation of nonlinear electromagnetic waves and enhanced nonreciprocity using transmissive space-time-coding metasurface," *Advanced Science*, Vol. 9, No. 11, 2105960, 2022.

[60] He, C., A. Cao, J. Chen, X. Liang, W. Zhu, J. Geng, and R. Jin, "Direction finding by time-modulated linear array," *IEEE Transactions on Antennas and Propagation*, Vol. 66, No. 7, 3642–3652, 2018.

[61] Li, G., S. Yang, and Z. Nie, "Direction of arrival estimation in time modulated linear arrays with unidirectional phase center motion," *IEEE Transactions on Antennas and Propagation*, Vol. 58, No. 4, 1105–1111, Apr. 2010.

[62] Tennant, A. and B. Chambers, "A two-element time-modulated array with direction-finding properties," *IEEE Antennas and Wireless Propagation Letters*, Vol. 6, 64–65, 2007.

[63] He, C., X. Liang, Z. Li, J. Geng, and R. Jin, "Direction finding by time-modulated array with harmonic characteristic analysis," *IEEE Antennas and Wireless Propagation Letters*, Vol. 14, 642–645, 2014.

[64] Dai, J. Y., J. Zhao, Q. Cheng, and T. J. Cui, "Independent control of harmonic amplitudes and phases via a time-domain digital coding metasurface," *Light: Science & Applications*, Vol. 7, No. 1, 90, 2018.

[65] Chen, J., W. Wang, C. He, Y. Li, X. Liang, J. Geng, and R. Jin, "Direction finding based on time-modulated array with multiharmonic analysis," *IEEE Transactions on Antennas and Propagation*, Vol. 68, No. 7, 5753–5758, 2020.

[66] Fang, X., M. Li, J. Han, D. Ramaccia, A. Toscano, F. Bilotti, and D. Ding, "Accurate direction-of-arrival estimation method based on space-time modulated metasurface," *IEEE Transactions on Antennas and Propagation*, Vol. 70, No. 11, 10 951–10 964, 2022.

[67] Bai, L., H. Cao, T. Bai, and C. He, "1-bit programmable metasurface-based 2-D direction finding," *IEEE Antennas and Wireless Propagation Letters*, Vol. 22, No. 9, 2160–2164, 2023.

[68] Wang, X. and C. Caloz, "Direction-of-arrival (DOA) estimation based on spacetime-modulated metasurface," in *2019 IEEE International Symposium on Antennas and Propagation and USNC-URSI Radio Science Meeting*, 1613–1614, Atlanta, GA, USA, Jul. 2019.

[69] Chen, X. Q., L. Zhang, S. Liu, and T. J. Cui, "Artificial neural network for direction-of-arrival estimation and secure wireless communications via space-time-coding digital metasurfaces," *Advanced Optical Materials*, Vol. 10, No. 23, 2201900, 2022.

[70] Turalchuk, P. A., "Direction of arrival estimation for retrodirective Rotman lens antenna array," in *Journal of Physics: Conference Series*, Vol. 1092, No. 1, 012157, 2018.

[71] Lin, Y.-Y. and W.-J. Liao, "A real-time/low-cost DOA estimation system based on Rotman lens array antenna," in *2016 IEEE 5th Asia-Pacific Conference on Antennas and Propagation (APCAP)*, 81–82, Kaohsiung, Taiwan, 2016.

[72] Hwang, M., D. An, S. Chang, Y. Youn, D. Kim, C. Lee, and W. Hong, "Demonstration of millimeter-wave reconfigurable intelligent surface (RIS) with built-in sensors for automatic tracking of direction-of-arrival (DOA)," *IEEE Sensors Letters*, Vol. 7, No. 8, 7003704, 2023.

[73] Ohmae, A. and S. Yagitani, "Direction-of-arrival estimation with planar Luneburg lens and waveguide metasurface absorber," *IEEE Access*, Vol. 11, 21 968–21 976, 2023.